

See discussions, stats, and author profiles for this publication at: <https://www.researchgate.net/publication/50248340>

The Role of Multifunctional Kinetics during Early-Stage Silicon Hydride Pyrolysis: Reactivity of Si₂H₂ Isomers with SiH₄ and Si₂H₆

ARTICLE in THE JOURNAL OF PHYSICAL CHEMISTRY A · MARCH 2011

Impact Factor: 2.69 · DOI: 10.1021/jp1118376 · Source: PubMed

CITATIONS

2

READS

39

2 AUTHORS, INCLUDING:



Andrew Adamczyk

Independent Researcher

14 PUBLICATIONS 163 CITATIONS

SEE PROFILE

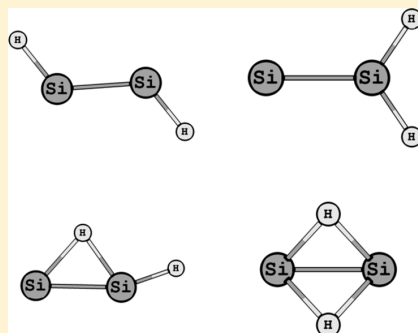
The Role of Multifunctional Kinetics during Early-Stage Silicon Hydride Pyrolysis: Reactivity of Si_2H_2 Isomers with SiH_4 and Si_2H_6

Andrew J. Adamczyk and Linda J. Broadbelt*

Department of Chemical and Biological Engineering, Northwestern University, 2145 Sheridan Road, Tech E136, Evanston, Illinois, United States 60208-3120

 Supporting Information

ABSTRACT: Kinetic parameters for the dominant pathways during the addition of the four Si_2H_2 isomers, i.e., *trans*-HSiSiH, SiSiH₂, Si(H)SiH, and Si(H₂)Si, to monosilane, SiH_4 , and disilane, Si_2H_6 , have been calculated using G3//B3LYP, statistical thermodynamics, conventional and variational transition state theory, and internal rotation corrections. The direct addition products of the multifunctional Si_2H_2 isomers were monofunctional substituted silylenes, hydrogen-bridged species, and silenes. During addition to monosilane and disilane, the SiSiH₂ isomer was found to be most reactive over the temperature range of 800 to 1200 K. Revised parameters for the Evans–Polanyi correlation and a representative pre-exponential factor for multifunctional silicon hydride addition and elimination reaction families under pyrolysis conditions were regressed from the reactions in this study. This revised kinetic correlation was found to capture the activation energies and rate coefficients better than the current literature methods.



INTRODUCTION

The four Si_2H_2 isomers on the singlet potential energy surface, i.e., *trans*-HSiSiH, SiSiH₂, Si(H)SiH, and Si(H₂)Si, have been suggested as precursor molecules to silicon wafer growth during silicon hydride pyrolysis (Figure 1).^{1–7} The geometries of and the pathways for the isomerization between the four isomers have been studied extensively.^{8–16} These relatively unstable and unsaturated silicon hydride species can potentially contribute to gas-phase silicon nanoparticle nucleation due to high reactivity. A detailed understanding of the microkinetics for the nucleation of silicon hydrides will allow for the improvement of applications in which silicon nanoparticles are desired or side products such as biological imaging¹⁷ and chemical vapor deposition (CVD), respectively.^{1,18,19} Pyrolysis of the feed gas, typically SiH_4 or Si_2H_6 , is a standard protocol to create polycrystalline or amorphous silicon nanoparticles in the gas phase or controlled growth of silicon wafers at a gas–solid interface. Si_2H_2 isomers are the simplest multifunctional silicon hydrides, i.e., these molecules contain multiple functionality by way of divalent silicon centers and/or Si–Si bonds with bond orders greater than one. These simple multifunctional silicon hydrides can be used as model chemical species to probe the nature of the reactive center with multifunctionality to determine if multifunctional kinetics follow the reaction family concept. Si_2H_2 isomers may play a critical role in the early stages of silicon nanoparticle nucleation, and filling the gap in knowledge for the reactivity of multifunctional silicon hydrides under pyrolytic conditions is needed.

Multifunctional silicon hydrides are less stable than saturated silicon hydrides or monofunctional silicon hydrides.²⁰ Comprehensive information about the reactivity of the four Si_2H_2 isomers

with another Si_2H_2 molecule (dimerization), H_2 in the gas phase, or at gas–solid interfaces is scant. Experimental and theoretical kinetic parameters are available for select dimerization reactions,²¹ addition and elimination reactions between Si_2H_2 isomers and H_2 ,^{22–26} and gas–solid interfacial reactions of the Si(H₂)Si and *trans*-HSiSiH isomers.²⁷ The study of reaction kinetics with closed-shell silicon hydrides under pyrolytic conditions has not been undertaken to the best of our knowledge. Experimental work in the area of low-temperature decomposition of saturated silicon hydrides suggests that Si_2H_2 is not reactive with H_2 , SiH_4 , Si_2H_6 , and CH_4 .²¹ However, the detailed mapping of the reaction kinetics of Si_2H_2 isomers has not been explored, and this reactivity information is critical when constructing detailed microkinetic models describing the nucleation of silicon nanoparticles which currently do not explicitly account for multifunctional kinetics beyond one representative Si_2H_2 isomer.^{18,19}

This study examines the addition reactions of the four Si_2H_2 isomers to closed-shell silicon hydrides, SiH_4 and Si_2H_6 (Figure 2 and Figure 3). All single events studied involved multifunctional compounds, i.e., molecules containing two divalent centers or both a divalent center and a double bond adjacent to the reactive center, and their mono- and dibridged stabilized forms. The composite method of G3//B3LYP²⁸ was used to calculate the electronic energy, and then statistical thermodynamics and internal rotation corrections^{29–37} were applied to all reactants

Received: December 13, 2010

Revised: February 8, 2011

Published: March 01, 2011

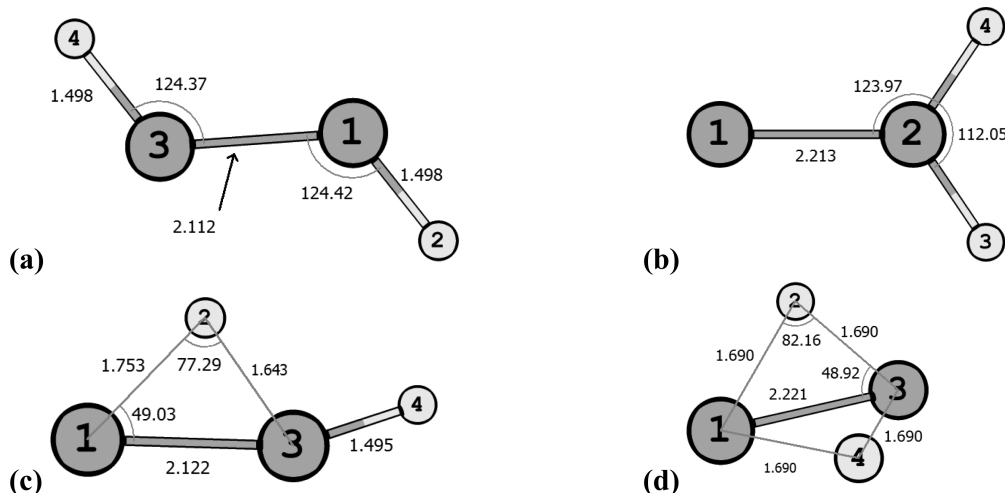


Figure 1. B3LYP/6-31G(d)-optimized geometries for the four isomers of Si_2H_2 . Distances are in angströms.

and transition states to incorporate temperature effects. Rate coefficients at 1 atm and 800–1200 K were calculated using conventional or variational transition state theory, and then activation energies, E_a , and single-event pre-exponential factors, \tilde{A} , were regressed. The rate-determining step was located for addition reactions that pass through a stable intermediate (or adduct), and then kinetic parameters for the overall reaction were calculated to align better with mechanistic modeling efforts. The reaction family concept was evaluated in the context of multifunctional silicon hydride kinetics. Lastly, revised parameters for the Evans–Polanyi correlation and two representative pre-exponential factors were developed for multifunctional silicon hydride addition and elimination reaction families under pyrolysis conditions.

COMPUTATIONAL METHODOLOGY

Quantum chemical calculations were performed with Gaussian 03.³⁸ All electronic energies for Si_2H_2 isomers, substituted silylenes, silenes, hydrogen-bridged intermediates, and transition states were calculated using the G3//B3LYP method,²⁸ which uses B3LYP geometries and higher-level corrections based on single point energies. The G3//B3LYP method was chosen for this theoretical study based on its very good agreement with Weizmann-1 (W-1) calculations³⁹ that were performed for the four major monofunctional reaction families of silicon hydride pyrolysis that are described in detail elsewhere.^{40–43} The saturated silicon hydrides of this study exist in the singlet state; however, an unsaturated silicon hydride such as Si_2H_2 can exist in either the singlet or the triplet state.^{11,12} Using the G3//B3LYP method, triplet-singlet splitting values of the four Si_2H_2 isomers were calculated (Table 1). These calculated triplet-singlet splitting values suggest that the singlet potential energy surface for Si_2H_2 addition and elimination is significantly lower in energy (i.e., ranging from 10.7 to 47.4 kcal mol⁻¹) than the mixed triplet-singlet potential energy surface despite different degrees of triplet state stabilization. Thus, for all results reported, the electronic wave functions for Si_2H_2 isomers, substituted silylenes, silenes, hydrogen-bridged intermediates, and transition states were optimized in the singlet state and tested for electronic wave function stability.^{44,45} Geometries and harmonic frequencies of the lowest energy conformations of all the species were determined at the B3LYP/6-31G(d) level. The harmonic frequencies

and zero-point energy (ZPE) were scaled by factors of 0.96 and 0.98, respectively, to account for anharmonicity in the normal vibrational modes as suggested by Scott and Radom.⁴⁶ The Cartesian coordinates and unscaled frequencies for all Si_2H_2 isomers, substituted silylenes, silenes, hydrogen-bridged intermediates, and only the rate-determining transition states (i.e., in the case of reactions 2 and 6 where there were two barriers, the first step in the Si_2H_2 addition direction was the rate-determining step) can be found in the Supporting Information.

Using conventional statistical thermodynamics, molecular partition functions based on the harmonic oscillator and rigid rotor approximations were used to calculate thermodynamic and kinetic properties as a function of temperature. Internal rotations that were more appropriately treated as free rotors under pyrolysis conditions that do not cancel between the reactant(s) and the transition state were quantified using free rotor approximations. This procedure was performed automatically using the CalcK script developed by our group.³³

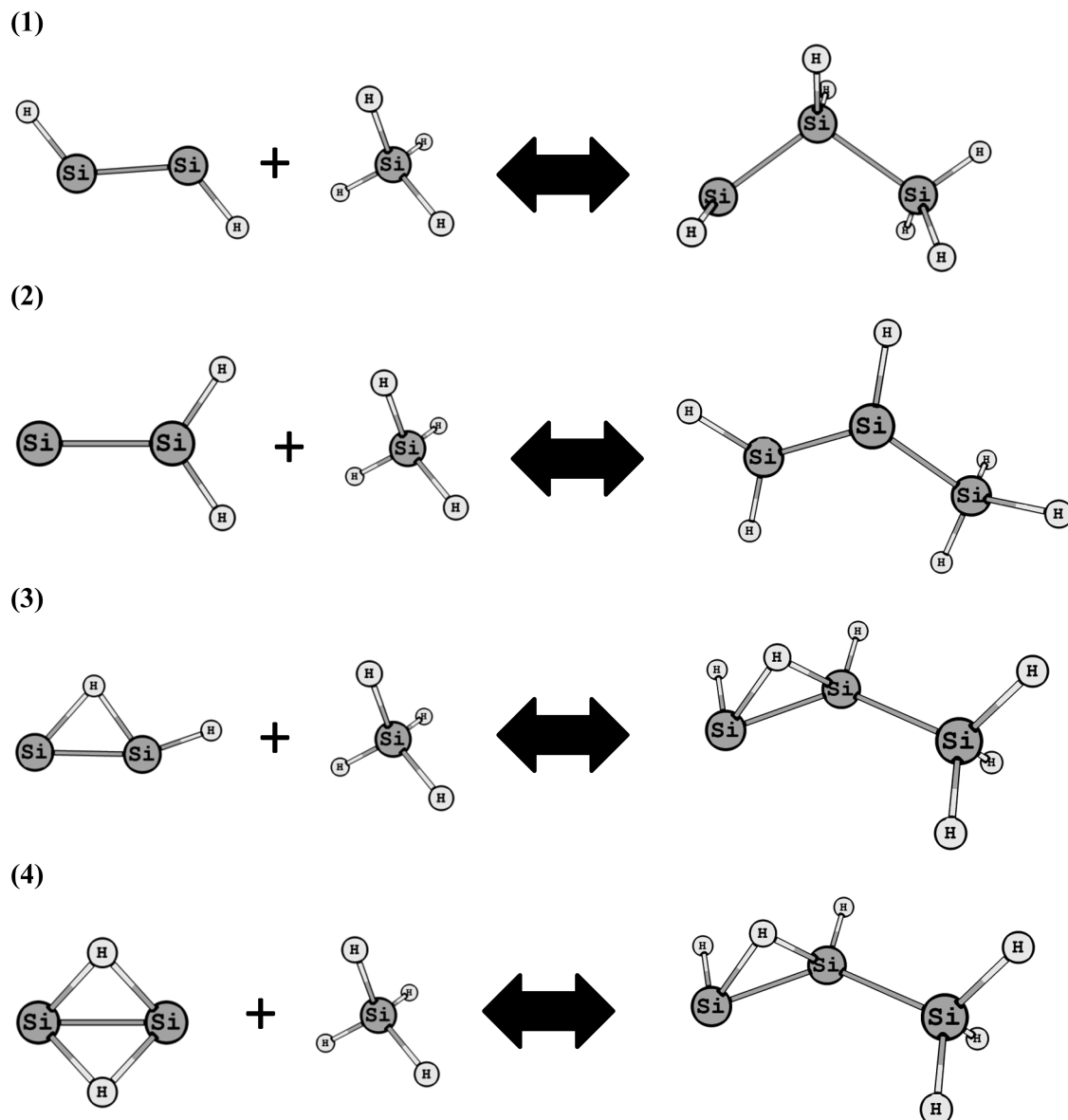
Transition states for the rate-determining step were found using the potential energy surface interpolation method QST3 and the climbing image nudged elastic band (CI-NEB) method.^{47–49} The imaginary frequency of each transition state was animated, and intrinsic reaction coordinate following was carried out to confirm that the normal vibrational mode pertained to the reaction coordinate of interest. Conventional TST⁵⁰ was then used to calculate rate coefficients according to the macroscopic formulation in eq 1 at 1 atm assuming an ideal gas:

$$k^{\text{TST}}(T) = \tilde{n}_d \tilde{k} = n_d \Lambda \exp\left(\frac{\Delta S^\ddagger}{R}\right) \exp\left(\frac{-\Delta H^\ddagger}{RT}\right) \quad (1)$$

where Λ is defined in eq 2:

$$\Lambda = \kappa(T) \frac{k_B T (V_m^0)^{-\Delta n}}{h} \quad (2)$$

where \tilde{k} is the single-event rate coefficient, $\kappa(T)$ is the Wigner tunneling correction⁵¹ at temperature T , k_B is Boltzmann's constant, h is Planck's constant, V_m^0 is the standard molar volume, R is the ideal gas constant, ΔS^\ddagger is the entropy of activation, ΔH^\ddagger is the enthalpy of activation, Δn is the change in the number of moles going from the reactant to the transition

Figure 2. Addition reactions for the four isomers of Si_2H_2 and monosilane.Table 1. G3//B3LYP Triplet–Singlet Splitting Values for the Four Isomers of Si_2H_2

Si_2H_2 isomer structure	G3//B3LYP electronic energies with zero-point vibrational energies		
	spin multiplicity		triplet–singlet splitting (kcal mol^{-1})
singlet (Hartrees)	triplet (Hartrees)		
<i>trans</i> -HSiSiH	−579.779984	−579.762865	10.7
SiSiH_2	−579.784733	−579.767218	11.0
$\text{Si}(\text{H})\text{SiH}$	−579.790683	−579.748888	26.2
$\text{Si}(\text{H}_2)\text{Si}$	−579.804446	−579.728880	47.4

state (i.e., zero for unimolecular elimination and -1 for bimolecular addition), and n_d is the reaction path degeneracy, or number of single events.⁵² ΔH^\ddagger and ΔS^\ddagger are calculated using standard formulas with internal rotation corrections taken into account.⁵⁰ Additionally, one-dimensional variational transition state theory^{9,53} was used to determine the rate coefficient of the

first step in the SiSiH_2 addition direction for reactions 2 and 6, and kinetic analysis was performed to identify the rate-determining step of the two-step addition.

The reaction path degeneracy, n_d , definition is based upon the symmetry of the reactant(s) and the transition state. The symmetry numbers for the species examined in this study can

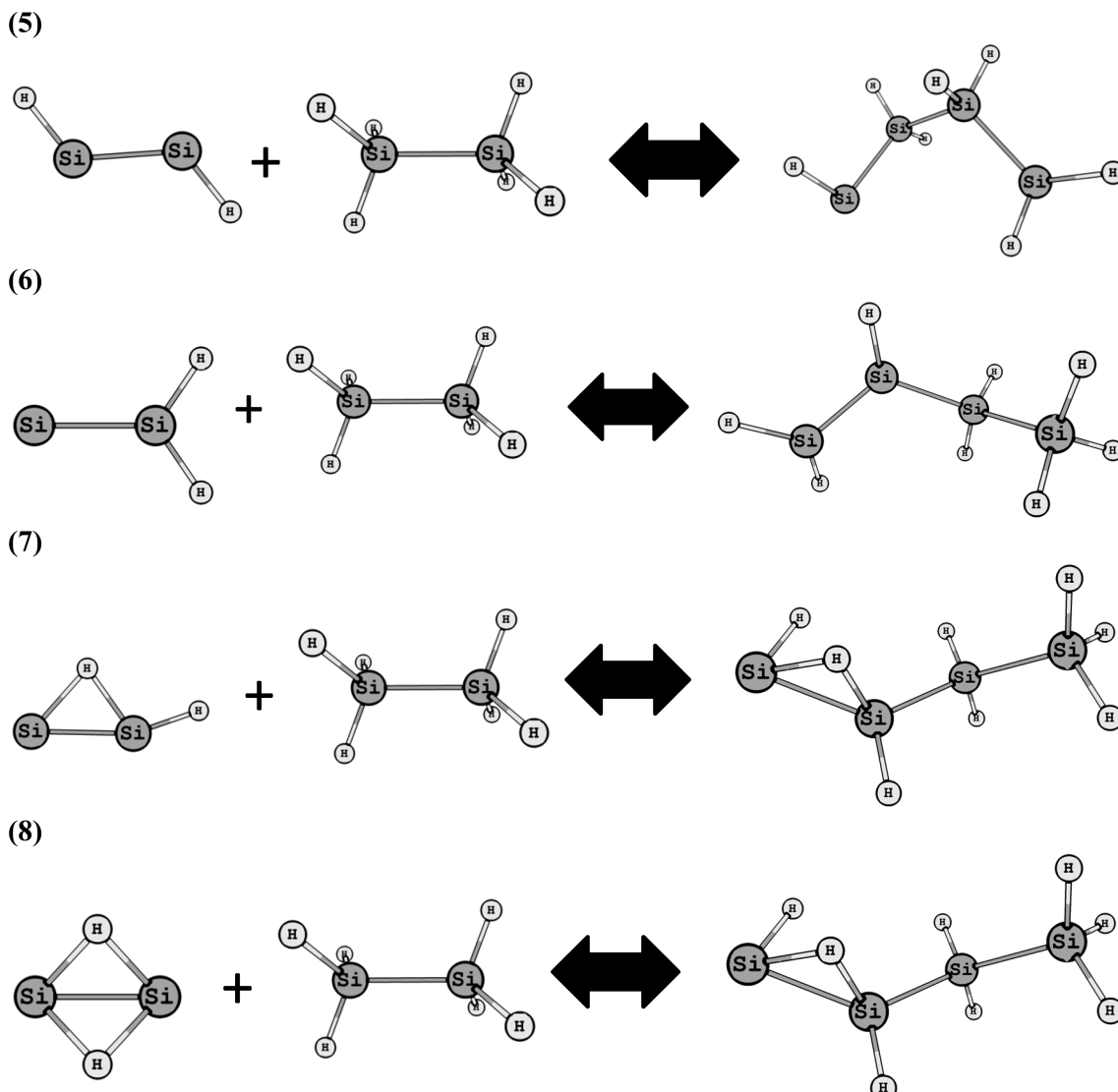


Figure 3. Addition reactions for the four isomers of Si_2H_2 and disilane.

be found in the Supporting Information. The reaction path degeneracies for this study follow eq 3:

$$n_d = \frac{n_{\text{chiral}}^{\ddagger}}{\prod_j n_{\text{chiral}}^{\text{reactant},j}} \times \frac{\prod_j \sigma^{\text{reactant},j}}{\sigma^{\ddagger}} \quad (3)$$

where n_{chiral} is the number of chiral isomers for the transition state and reactant(s), and σ is a product of the external rotational symmetry numbers for the transition state and reactant(s). Internal symmetry numbers for noncanceling internal rotations treated as free rotations were included in the free rotor partition functions.

For elimination reactions involving the SiSiH_2 isomer, statistical thermodynamics defines the apparent rate coefficient as eq 4, when two barriers are connected by a stable adduct and equilibrium of the first step in the SiSiH_2 elimination direction is assumed:

$$k_{\text{apparent}} = k_{\text{reactants-adduct}}^{\text{TST}} K_{\text{adduct-product}} \quad (4)$$

where K is the equilibrium constant derived from molecular partition functions. K is unitless for thermodynamic equilibrium between the adduct and product silicon hydride. The units for k_{apparent} are the same as for k^{TST} for elimination reactions and derived from the pre-exponential factor defined in eqs 1 and 2.

The single-event parameters of the Arrhenius relationship, \tilde{A} and E_a , were obtained by fitting $\ln k$ versus T^{-1} over the temperature range 800–1200 K. This procedure was performed automatically using the *CalcK* script developed by our group.³³ Arrhenius behavior was very nonlinear over the larger temperature range of 298–1500 K, and thus a reduced temperature range was used to ensure a good linear fit for Arrhenius parameter regression. Over the reduced temperature range of 800–1200 K that is most relevant to pyrolysis conditions, reaction 1 had linear regression coefficients equal to 0.99 and 1 for the addition and elimination reactions, respectively. The most nonlinear Arrhenius plots were for reactions 2 and 6 which had linear regression coefficients equal to 0.96 and 0.91 for SiSiH_2 addition reactions, respectively.

One common method for predicting E_a is the Evans–Polanyi correlation⁵⁴ depicted in eq 5, where E_0 and α are parameters

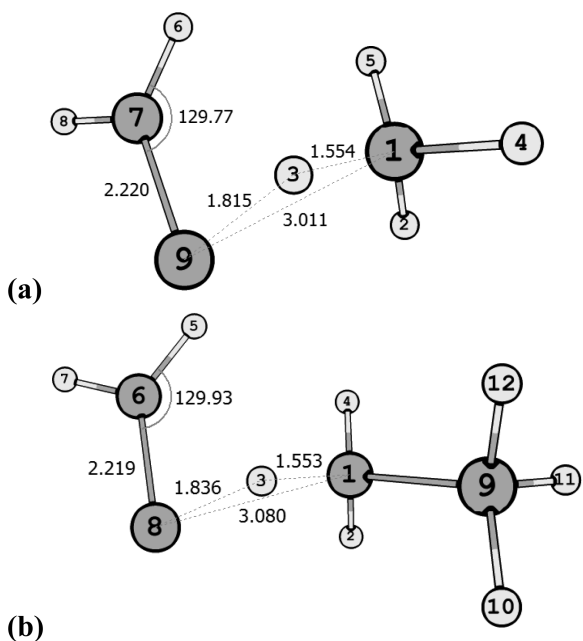


Figure 4. B3LYP/6-31G(d)-optimized geometries for the adducts formed during SiSiH_2 addition to (a) SiH_4 and (b) Si_2H_6 . Distances are in angströms.

that are determined from linear regression against experimental or theoretical values and are constant for a given reaction family.

$$E_a = E_0 + \alpha \Delta H_{\text{rxn}} \quad (5)$$

where α is the unitless transfer coefficient, E_0 is the intrinsic barrier of the reaction, and ΔH_{rxn} is the standard enthalpy of reaction. ΔH_{rxn} is calculated using standard formulas⁵⁰ or collected from experiment. To obtain this linear regression, the sum of the two transfer coefficients was fixed to be equal to one, i.e., $\alpha_{\text{addition}} + \alpha_{\text{elimination}} = 1$, and the intrinsic barrier, E_0 , for the addition and elimination reactions were constrained to be equal. The principle of enthalpic consistency is explained by examining the relationship $E_a = \Delta H^\ddagger + (\Delta n)RT$ from transition state theory.⁵⁵ This equation with algebraic manipulation reveals that for addition and elimination reaction pairs of reactions in the Si_2H_2 addition and elimination reaction family, the sum of the transfer coefficients is equal to unity.

RESULTS AND DISCUSSION

Presence of an Adduct. Intermediates with hydrogen-bridging are common in silicon hydride chemistry and hydrides of other group 13 and 14 elements.^{56–60} It is important to first distinguish the presence of intermediates with intra- or intermolecular hydrogen-bridging. The former is more readily formed and will occur faster than intermolecular hydrogen-bridging (or adduct formation as observed for reactions 2 and 6 of Figure 2 and Figure 3) since this transformation does not require the precise collision of two molecules with correct orientation in the gas phase. $\text{Si}(\text{H})\text{SiH}$ and $\text{Si}(\text{H}_2)\text{Si}$ are grouped under hydrogen-bridged species that are formed due to intramolecular hydrogen-bridging or isomerization. The isomerization barriers between the four Si_2H_2 isomers are discussed in detail elsewhere (see Introduction). This section will focus upon adducts (or intermolecular intermediates) formed between SiSiH_2 and saturated silicon hydrides.

Mapping of the Si_2H_2 addition and elimination reaction potential energy surfaces for two of the reactions, i.e., reactions 2 and 6, showed passage through an adduct, which is a stable 1,2-bridged species as depicted in Figure 4 for Si_2H_2 addition to SiH_4 and Si_2H_6 . Analysis of Wiberg bond indices⁶¹ in the adduct(s) revealed a bond order of approximately two for the $\text{Si}–\text{Si}$ bond of the SiSiH_2 segment of the adduct. The lone electron pair for SiSiH_2 , which contributes to the multifunctional nature of this isomer, is not in the highest occupied molecular orbital (HOMO) and consequently does not participate as a frontier molecular orbital in the reaction (Figure 5). To the best of our knowledge, there is no experimental evidence for the intermolecular formation of an adduct for Si_2H_2 addition and elimination reactions; however, there is experimental evidence for the intermolecular formation of a hydrogen-bridged intermediate for the reaction of silylene and monosilane to form disilane by Becerra et al.⁶² and the intramolecular formation of a hydrogen-bridged intermediate for the isomerization of silylsilylene to disilene by McCarthy et al.⁶³ A summary of the enthalpies of reaction at 800 K and 1 atm for the conversion of the reactants into the adduct and the conversion of the adduct into the product silene are summarized for reactions 2 and 6 in Table 2. Intrinsic reaction coordinate following confirms the absence of an adduct for the remaining reactions of this study. Each of these remaining reactions does not have a vacant low energy p orbital in the Si_2H_2 isomer for electron pair acceptor behavior (Figure 5). This behavior is contrary to monofunctional silylenes or silylenes with multiple functionality remote from the reactive center, which easily form adducts due to a vacant low energy p orbital.⁶⁴

The formation of an adduct from the separated reactants is always exothermic, and no significant enthalpic barrier was observed for any of the reactions involving the SiSiH_2 isomer under pyrolysis conditions. The enthalpy of reaction at 800 K and 1 atm for this addition averaged $-9.0 \text{ kcal mol}^{-1}$, where the more exothermic enthalpy of reaction was $-9.4 \text{ kcal mol}^{-1}$ for reaction 6, i.e., the formation of an adduct from SiSiH_2 and disilane. The conversion of the adduct to a silene is also very exothermic, revealing that the adduct is enthalpically uphill from the silene product. The enthalpy of reaction at 800 K and 1 atm for the conversion of the adduct to a silene exceeded $-30 \text{ kcal mol}^{-1}$ for both of the reactions.

Internal Rotation Corrections. Vibrational modes that were more appropriately treated as free rotations that do not cancel out between the reactant(s) and the transition state (e.g., *trans*-HSiSiH addition to monosilane has two potential internal rotations about the donor silicon atom and donor hydrogen atom and the divalent center of *trans*-HSiSiH and the donor hydrogen atom in the transition state that are not present in the product) were treated using a one-dimensional internal rotation model. These potential internal rotations can be viewed in Figure 8a as the bonds formed by atoms 3–1 and 3–6, respectively. For *trans*-HSiSiH addition to monosilane, the potential internal rotations in the product silylene are about the silicon–silicon σ bond formed and the silicon–silicon σ bond formed from the higher order bond in *trans*-HSiSiH that now has a bond order near 1. The remaining three isomers, i.e., SiSiH_2 , $\text{Si}(\text{H})\text{SiH}$, and $\text{Si}(\text{H}_2)\text{Si}$, exhibit two noncanceling internal rotations in the transition state and only one internal rotation about the silicon–silicon σ bond formed in the product.

To assess the magnitude of the effects of internal rotation, potential energy scans at the B3LYP/6-31G(d) level of theory were performed on the internal rotations that did not cancel out

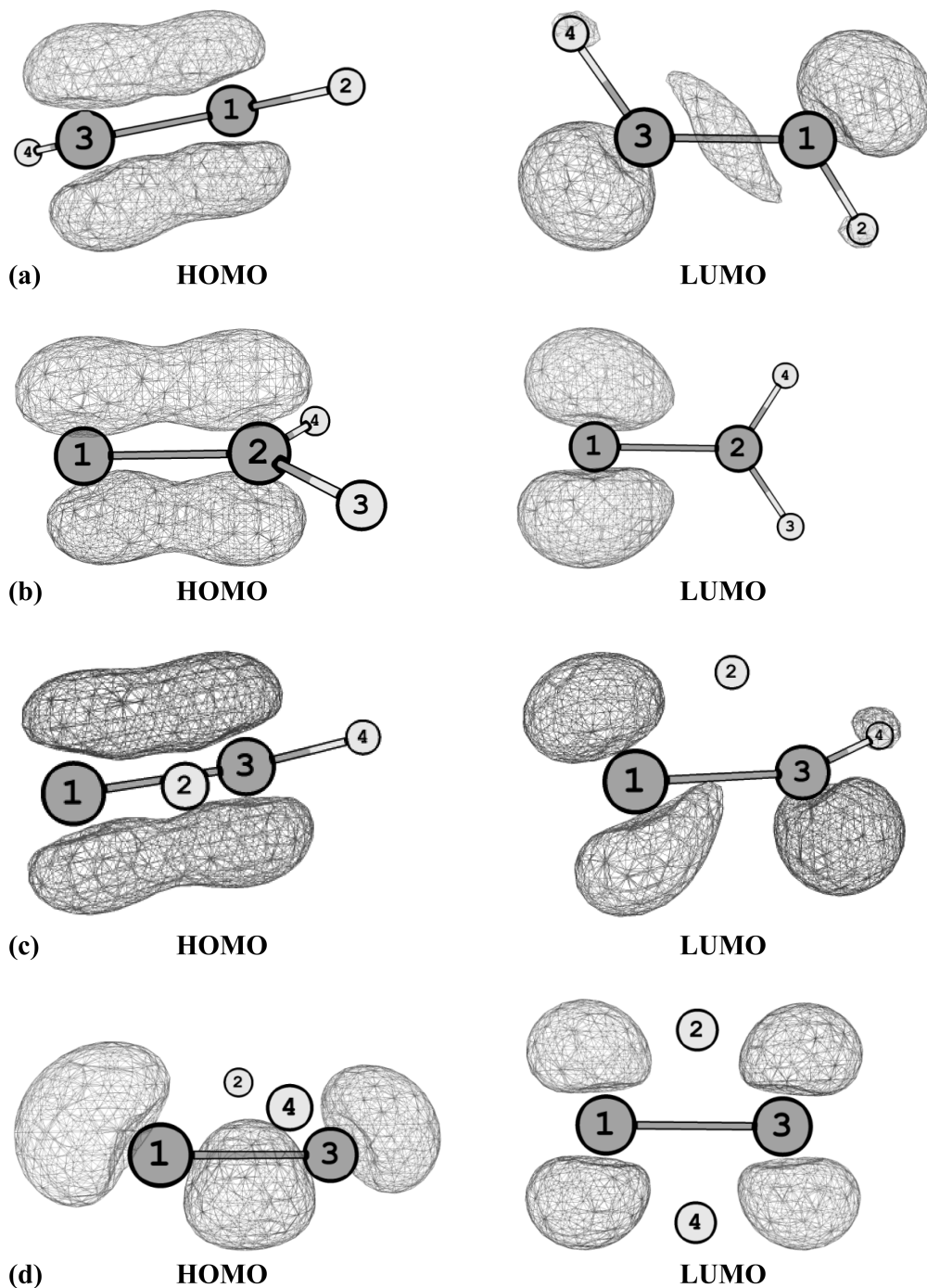


Figure 5. Frontier molecular orbitals for the four isomers of Si_2H_2 from B3LYP/6-31G(d): (a) trans -HSiSiH, (b) SiSiH_2 , (c) $\text{Si}(\text{H})\text{SiH}$, and (d) $\text{Si}(\text{H}_2)\text{Si}$. The molecular orbitals depicted have a 0.075 contour value for each species. HOMO is the highest occupied molecular orbital of the isomer, and LUMO is the lowest unoccupied molecular orbital of the isomer.

for all of the reactions in this study. For the transition state of reaction 1 (Figure 8a), internal rotations about 3–6 and 3–1 were examined independently. The vibrational frequencies primarily associated with the internal rotations about 3–6 and 3–1 were animated, and some degree of coupling of these two internal rotations was observed. However, given the computational expense required for a coupled two-dimensional treatment of these internal rotations,^{65–67} these calculations were deemed beyond the scope of this study. The rotation about 3–6 was found to have a significant barrier, and the harmonic oscillator

approximation is thus valid for this torsional mode. In contrast, the internal rotation about the bond connecting atoms 3–1 is better approximated by the hindered rotor model at low temperatures and the free rotor model at higher temperatures. An approximate solution using the product of the uncoupled one-dimensional free rotor partition function for the 3–1 rotation, which was an appropriate choice at the temperatures of interest in this study, and the harmonic oscillator partition function for the 3–6 rotation was employed. The internal rotations in the product silane were found to have very low barriers to rotation,

Table 2. Enthalpy of Reaction at 800 K and 1 atm for Formation of the Adduct from SiSiH_2 and Silane Reactants (step 1) and Conversion of the Adduct To Form the Product Silene (step 2)

reaction	$\Delta H_{\text{rxn}}^{800}$ (kcal mol ⁻¹)	
	step 1	step 2
2	-8.6	-30.9
6	-9.4	-32.7

and the free rotor approximation is valid. The transition from a hindered to a free rotor was assumed to occur at the temperature at which $k_B T$ equals the maximum barrier height to internal rotation, and, under the conditions of pyrolysis, the assumption of free rotors is valid for the torsional modes that are better approximated as internal rotations. On the basis of the fact that these internal rotation corrections had an appreciable effect on the rate coefficients for reaction 1, all the reactions in this study were treated using the same approach (i.e., the transition state internal rotation about the donor silicon atom and donor hydrogen atom and the product silicon hydride internal rotation about the silicon–silicon σ bond(s) formed were approximated as free rotors).

The effects of internal rotation corrections on the rate coefficients and Arrhenius parameters for all the Si_2H_2 addition and elimination reactions are summarized in Table 3. For reactions 2 and 6, the first barrier in the addition direction was assumed to be the rate-determining step in calculating the rate coefficients (see Rate-Determining Step). Internal rotation corrections change the overall rate coefficients for both the Si_2H_2 addition and elimination reactions by average absolute factors of 2.8 and 4.1 at 1000 K and 1 atm, respectively. The largest changes in the rate coefficients for the Si_2H_2 addition and elimination reactions were observed for reactions 2 and 5, respectively. The \tilde{A} and E_a values changed by an absolute factor of 3.8 and decreased by 0.9 kcal mol⁻¹, respectively, on average for the Si_2H_2 addition reactions, while the \tilde{A} and E_a values changed by an absolute factor of 3.5 and decreased by 0.2 kcal mol⁻¹, respectively, for the Si_2H_2 elimination reactions.

Rate-Determining Step. The adduct is stable for reactions 2 and 6, but it is cumbersome to have to track it explicitly in mechanistic models, since schemes for predicting the properties of these intermediates are not available. It is more convenient to consolidate the two-step conversion of SiSiH_2 and the saturated silane to a product silene and its reverse reaction into one overall transformation. Prior to consolidation of the two-step conversion, the rate-determining step was first validated by monitoring the reaction dynamics of reactions 2 and 6. Three microkinetic models were created assuming (1) a full model, (2) that the second step is rate-determining, and (3) that the first step is rate-determining. Model 1 explicitly includes the kinetic parameters for both reaction steps without assuming a rate-determining step. The rate coefficient for the barrierless step to form the adduct from the reactants was calculated using one-dimensional variational transition state theory.^{9,53} The overall rate coefficient for model 2 was calculated as $k = K_1 k_2$, where K_1 is the equilibrium constant for the first step, and k_2 is the rate coefficient for the second step. Model 3 calculates the overall rate coefficient as $k = k_1$, where k_1 is the rate coefficient for the first step. Over the temperature range of 800–1200 K, model 3 is superior in predicting the reaction dynamics of the full model for reactions

2 and 6. When the temperature is above this range, model 2 outperforms model 3 for reactions 2 and 6, as the rate-determining step changes. Thus, SiSiH_2 addition and its reverse reaction were assumed to be controlled by the first step as the rate-determining step under pyrolysis conditions, i.e., 800–1200 K. Moreover, the adduct will be sufficiently stabilized over the temperature range of this study by collisions in the high-pressure limiting case where we are applying conventional transition state theory.⁶⁸ Figures of the product silene concentration as a function of time at 800 and 1200 K for reactions 2 and 6 using models 1 through 3, tables of rate coefficients calculated from G3//B3LYP over the temperature range of 800 to 1200 K for the full model and the reduced model 3, and potential energy surfaces for reactions 2 and 6 can be found in the Supporting Information.

Reactivity Analysis with Frontier Molecular Orbital Theory. The frontier molecular orbitals in a molecule or between reactants are largely responsible for their observed spectroscopic and chemical properties and reactivity, respectively. Frontier molecular orbital (FMO) theory⁶⁹ has been successfully implemented in hydrocarbon and monofunctional silicon hydride chemistry to develop linear correlations for the prediction of rate coefficients using $E_{\text{HOMO}} - E_{\text{LUMO}}$ energy gaps between the reactants.^{43,70,71} The theoretical investigation of reactivity with frontier molecular orbitals is valuable because the information generated can be used to discern information about reactions that may lack detailed knowledge about the transition state and the potential energy surface of reaction and reveal details about the change of the electronic distribution (or density) during reaction.⁷² More specifically, a theoretical study of the role of frontier molecular orbitals for multifunctional reaction kinetics will give insight into the balance of nucleophilic and electrophilic behavior of the attacking reactant in the transition state.

It is well-established that monofunctional silylenes form silylene–Lewis acid complexes (or adducts) and thereby behave largely as a Lewis acid during monofunctional addition reactions.⁶⁴ For multifunctional kinetics, the details about the change of the electronic distribution during reaction have not been explored to the best of our knowledge. Evidence supporting silylene behavior as a Lewis base is not widespread despite the fact that silylene has a lone electron pair and a vacant low energy orbital for electron pair donor or acceptor behavior, respectively. During an addition reaction between Si_2H_2 and a saturated silicon hydride, the bonding orbital of the saturated silicon hydride first approaches the Si_2H_2 isomer and through nucleophilic interaction donates electrons to the lowest occupied molecular orbital (LUMO) of the Si_2H_2 isomer (Figure S). When observing HOMO–LUMO interactions in silicon hydride chemistry, this attacking behavior of a closed shell species is consistent with the known tendency of hydrogen to scavenge bonds that have high bond order such as the silicon–silicon bonds in SiSiH_2 and *trans*-HSiSiH, which have Wiberg bond indices of 2.0 and 2.6, respectively.⁷³ The frontier molecular orbital energies of the four Si_2H_2 isomers and the saturated silicon hydride reactants, SiH_4 and Si_2H_6 , and the relative energy differences between reactants for all the Si_2H_2 addition reactions are summarized in Table 4. It is important to note that in nearly every case the reaction begins with the nucleophilic addition of the saturated silicon hydride to the unsaturated Si_2H_2 species, because the HOMO–LUMO energy gap between the HOMO of the saturated silicon hydride and LUMO of the Si_2H_2 isomer is generally lower than the HOMO–LUMO energy gap between the HOMO of the Si_2H_2 isomer and the LUMO of the saturated

Table 3. Relative Differences of Arrhenius Parameters and Rate Coefficients at 1000 K and 1 atm Showing the Effect of Internal Rotation Corrections for Addition and Elimination Reactions for the Four Isomers of Si_2H_2

reaction	addition			elimination		
	$A^{\text{IR}}/A^{\text{HO}}$	$E_a^{\text{IR}} - E_a^{\text{HO}}$, kcal mol ⁻¹	$k^{\text{IR}}/k^{\text{HO}}$ (1000 K)	$A^{\text{IR}}/A^{\text{HO}}$	$E_a^{\text{IR}} - E_a^{\text{HO}}$, kcal mol ⁻¹	$k^{\text{IR}}/k^{\text{HO}}$ (1000 K)
1	0.23	-0.91	0.37	1.86	-0.99	3.06
2	0.09	-0.93	0.14	0.16	-0.09	0.17
3	1.17	-0.67	1.65	2.57	0.18	2.35
4	0.54	-0.78	0.80	1.20	0.07	1.16
5	0.45	-0.94	0.72	7.24	-0.95	11.69
6	0.18	-0.95	0.29	0.24	-0.03	0.24
7	2.19	-0.82	3.31	3.72	0.11	3.52
8	0.66	-0.90	1.04	1.15	0.03	1.13

Table 4. Energy Differences between the Highest Occupied and Lowest Unoccupied Molecular Orbitals (E_{HOMO} and E_{LUMO} , respectively) at the B3LYP/6-31G(d) Level: (a) for the Si_2H_2 and Saturated Silicon Hydride Reactants Individually and (b) between the Reactants for all Si_2H_2 Addition Reactions^a

	(a)					
	reactant 1				reactant 2	
	<i>trans</i> -HSiSiH	SiSiH ₂	Si(H)SiH	Si(H ₂)Si	SiH ₄	Si ₂ H ₆
E_{HOMO}	-131	-129	-133	-133	-222	-187
E_{LUMO}	-82	-84	-50	-46	32	13
$\Delta E_{\text{HOMO-LUMO}}$	49	45	83	87	254	200

	(b)							
	reaction							
	1	2	3	4	5	6	7	8
$\Delta E_{\text{HOMO}(\text{silane})-\text{LUMO}(\text{Si}_2\text{H}_2)}$	-140	-138	-171	-176	-106	-104	-137	-142
$\Delta E_{\text{HOMO}(\text{Si}_2\text{H}_2)-\text{LUMO}(\text{silane})}$	-164	-161	-165	-165	-144	-142	-145	-145

^a Electronic energies are in kcal mol⁻¹.

silicon hydride. Contrary to hydrocarbon chemistry, the silicon atom is less electronegative than the hydrogen atom, and thus there will be a partial negative charge on the surrounding hydrogen atoms on saturated silicon hydrides that behave as potential nucleophiles during addition reactions. The Si_2H_2 addition and elimination reaction mechanism is further complicated because the Si_2H_2 isomers can exhibit both electrophilic and nucleophilic behavior. For instance, the interaction between the bonding orbital of SiH₄ and Si₂H₆ and the empty p orbital of the SiSiH₂ isomer is followed by nucleophilic attack of the SiSiH₂ isomer which donates electrons to the nonbonding orbital of SiH₄, thereby cleaving the Si–H bond on SiH₄ and forming a Si–H bond on the SiSiH₂ isomer.

Kinetic Parameters, the Reaction Family Concept, and Evans–Polanyi Correlations. Kinetic parameters, E_a and \tilde{A} , were regressed for the reactions of Figure 2 and Figure 3. This study concentrates on pyrolysis conditions and the impact of tunneling and above-the-barrier reflection is approximated by the Wigner tunneling correction. Furthermore, pressure dependence of the rate coefficient decreases in reacting systems with three or more silicon atoms, and pressure effects on reaction kinetics were ignored for all the reactions in this study. All of the reactions in Figure 2 and Figure 3 were treated using the same approach, and a summary of the zero-point corrected energy barriers, the regressed E_a and \tilde{A} values for the overall transformations, and

the enthalpies of reaction at 800 K and 1 atm for the formation of the direct products, i.e., silylenes, hydrogen-bridged species, and silenes, from the four Si_2H_2 isomers and reactant saturated silicon hydrides, SiH₄ and Si₂H₆, including internal rotation corrections are summarized in Table 5. In Figure 6 and Figure 7, the Arrhenius plots for all of the reactions in this study are depicted.

The Si_2H_2 isomers were found to be more reactive with Si₂H₆ than SiH₄ because the products formed from the addition to SiH₄ lack the electron delocalization and subsequent stabilization of the divalent center or double bond present in the larger products formed from the addition to Si₂H₆. The most reactive Si_2H_2 isomer with both SiH₄ and Si₂H₆ is SiSiH₂. The hydrogen-bridged isomers are notably less reactive, and their rate coefficients essentially differ by the respective reaction path degeneracies for each case. For instance, Si(H)SiH is found to be the least reactive isomer in both the reaction with SiH₄ and Si₂H₆ because the reaction path degeneracy is lower than the reaction path degeneracy for Si(H₂)Si. Each Si_2H_2 isomer will form a distinct type of product silicon hydride based upon structural similarities in the reactive center for a given Si_2H_2 isomer and the saturated silicon hydride substrate. The addition of the *trans*-HSiSiH isomer to a saturated silicon hydride will form silylenes while the addition of the SiSiH₂ isomer to a saturated silicon hydride will form silenes. The di-

Table 5. Arrhenius Parameters, Zero Point Energy Corrected Barriers, and Enthalpy of Reaction at 800 K and 1 atm^a

reaction	addition				elimination		
	E_o , kcal mol ⁻¹	$\log \tilde{A}$	E_a , kcal mol ⁻¹	ΔH_{rxn}^{800} , kcal mol ⁻¹	E_o , kcal mol ⁻¹	$\log \tilde{A}$	E_a , kcal mol ⁻¹
1	1.55	-11.63	5.25	-33.78	36.37	14.37	36.47
2	-2.73	-10.61	1.42	-40.15	37.93	14.67	39.17
3	9.29	-13.55	11.96	-26.71	36.12	12.63	36.26
4	14.28	-12.27	18.21	-16.94	32.48	12.80	32.68
5	-0.47	-11.63	3.39	-36.08	36.91	14.26	36.92
6	-3.37	-10.60	0.92	-42.79	40.16	14.54	41.31
7	5.84	-13.42	8.75	-30.22	36.42	12.52	36.58
8	11.35	-11.94	15.73	-20.45	33.29	12.89	33.73

^aThe kinetic parameters were calculated assuming that the second step in the addition direction is equilibrated for reactions 2 and 6. Å has units of cm³ molecule⁻¹ s⁻¹ and s⁻¹ for the addition and elimination reactions, respectively.

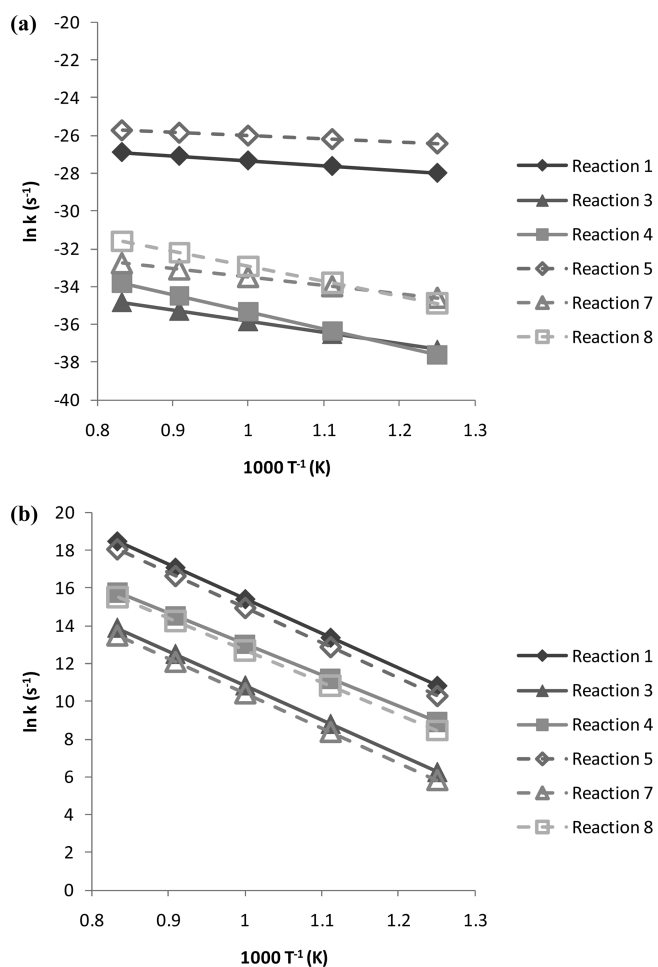


Figure 6. Arrhenius plots for the (a) addition and (b) elimination reactions of *trans*-HSiSiH, Si(H)SiH, and Si(H₂)Si.

monobridged isomers will both form monobridged species upon addition to a saturated silicon hydride. The primary product of Si(H₂)Si addition to a saturated silicon hydride will be a monobridged species because sustaining two simultaneous hydrogen bridges about one Si–Si bond is not favorable energetically for species beyond two silicon atoms. In silicon hydride chemistry, it is well accepted that hydrogen will scavenge higher order Si–Si bonds to lower the coordination

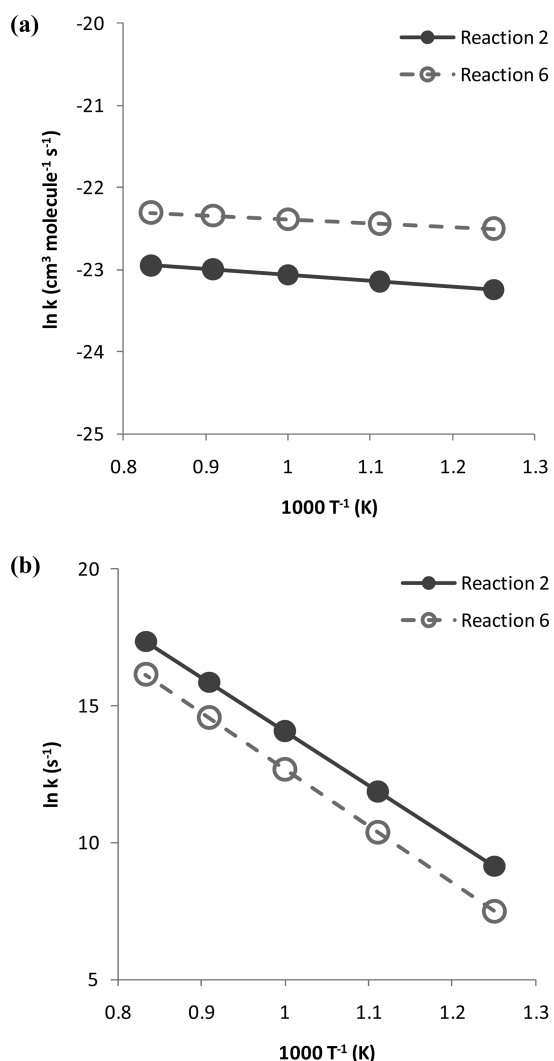


Figure 7. Arrhenius plots for the (a) addition and (b) elimination reactions of SiSiH₂.

number of a silicon atom to an ideal connectivity of four separate σ bonds. The formation of hydrogen-bridged products from hydrogen-bridged isomers, silene products from the SiSiH₂ isomer, and silylene products from the *trans*-HSiSiH isomer can be rationalized by observing the LUMO contour of

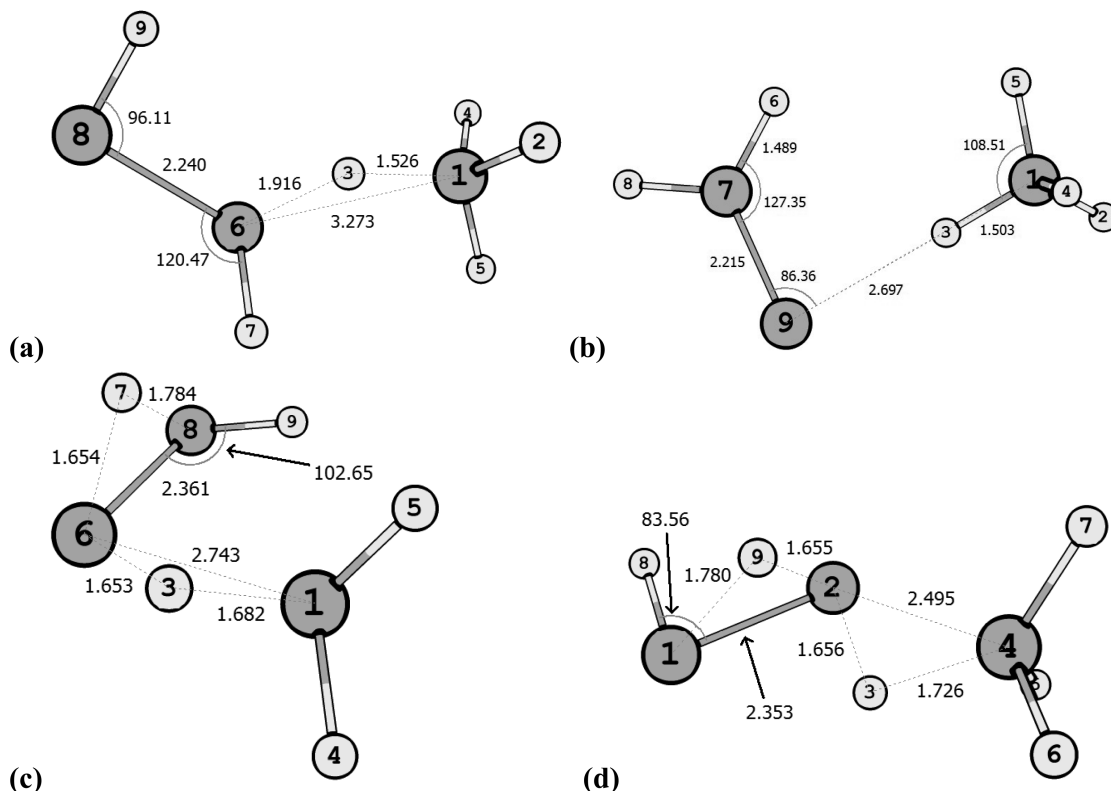


Figure 8. B3LYP/6-31G(d)-optimized rate-determining transition state geometries for the addition of the four isomers of Si_2H_2 to SiH_4 : (a) *trans*-HSiSiH, (b) SiSiH_2 , (c) $\text{Si}(\text{H})\text{SiH}$, and (d) $\text{Si}(\text{H}_2)\text{Si}$. Distances are in angströms.

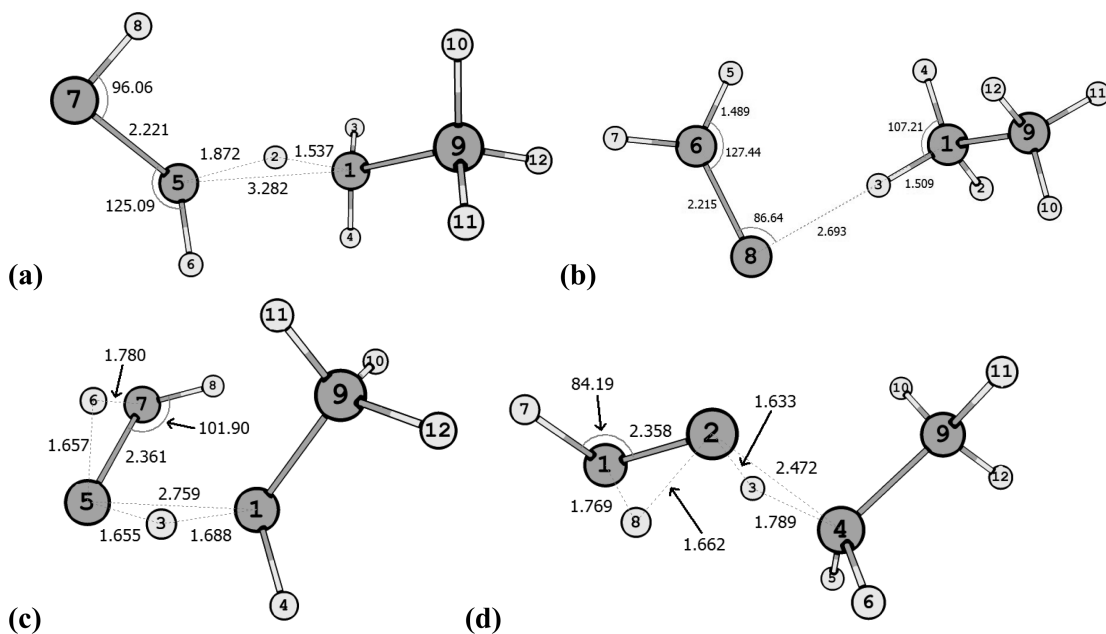


Figure 9. B3LYP/6-31G(d)-optimized rate-determining transition state geometries for the addition of the four isomers of Si_2H_2 to Si_2H_6 : (a) *trans*-HSiSiH, (b) SiSiH_2 , (c) $\text{Si}(\text{H})\text{SiH}$, and (d) $\text{Si}(\text{H}_2)\text{Si}$. Distances are in angströms.

the Si_2H_2 isomers in Figure 5. The participating frontier LUMO of each Si_2H_2 isomer shows precise positioning that is favorable for the overlap and subsequent formation of Si–Si σ bonds for a product silylene, hydrogen-bridged species, and silene for *trans*-HSiSiH, both bridged isomers, and SiSiH₂, respectively.

Rate coefficients for Si_2H_2 addition show both positive and negative temperature dependencies, depending on the temperature range of interest. Over the temperature range of this study, the addition of Si_2H_2 isomers to monosilane and disilane has positive activation energies, and classic Arrhenius behavior is

Table 6. Evans–Polanyi Parameters for Multifunctional Silicon Hydride Addition and Elimination Reaction Families Generalized from the Si_2H_2 Addition and Elimination Reactions in This Study

reaction family	α_{addition}	$\alpha_{\text{elimination}}$	E_0 , kcal mol ⁻¹
$\text{Si}_2\text{H}_2 + \text{Si}_n\text{H}_{n+2} \longleftrightarrow$ silene, 1,2-bridged species, or substituted silylene	0.71	0.29	29.1

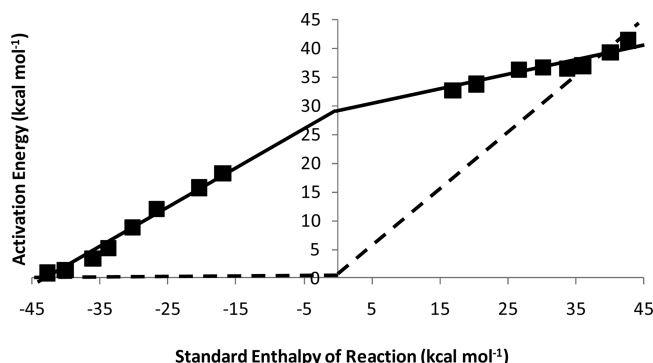


Figure 10. Plot of activation energy versus overall standard enthalpy of reaction (at 800 K) for the reactions shown in Figure 2 and Figure 3 (forward and reverse pairs). The solid lines are the best straight line fits to the overall activation energy with the parameters obtained from Table 6. Activation energies predicted by the current literature correlation for monofunctional substituted silylene addition and elimination reaction kinetics for silicon hydrides are shown as a function of standard enthalpy of reaction with a dashed line.

observed. Above the range of temperatures used in the linear regression for activation energies, the overall apparent activation energies for SiSiH_2 addition reactions become negative, as the rate-determining step for the formation of silenes in the addition direction becomes the second barrier. This reverse in classical Arrhenius behavior can play a critical role in controlling nanoparticle growth in the gas phase when coupling the reaction kinetics of silicon nanoparticle formation with reactor simulations composed of steep temperature gradients near the reactor inlet and outlet. For the elimination reaction, classic Arrhenius behavior is observed for all isomers and temperature ranges investigated.

Before the reaction family concept is applied, structural similarities or trends in the transition state geometry must be observed in a given reaction family and change uniformly with systematic changes in the substituents on the reactive center.^{74,75} Figure 8 and Figure 9 show the transition state geometries for the rate-determining step in the transformation of the Si_2H_2 isomer and saturated silicon hydride reactants to the product silicon hydride for the reactions of this study. Transition state geometries of the second step in the addition direction, which are not the rate-determining transition state geometries for reactions 2 and 6 over the temperature range of this study, can be found in the Supporting Information. The structural changes upon the addition of a silyl substituent to the reactive center can be observed by comparing these geometries. Si_2H_2 isomers with hydrogen-bridging, $\text{Si}(\text{H})\text{SiH}$ and $\text{Si}(\text{H}_2)\text{Si}$, exhibit the shortest Si–Si distance in the reactive center, i.e., the distance between atoms 2 and 4 in Figure 8d, due to the increased stability of the hydrogen-bridged Si_2H_2 isomer relative to the unbridged Si_2H_2 isomers (Figure 8c,d and Figure 9c,d). The tighter transition state for these more stable bridged isomers also imparts more instability of the transition state due to steric interactions. When acyclic

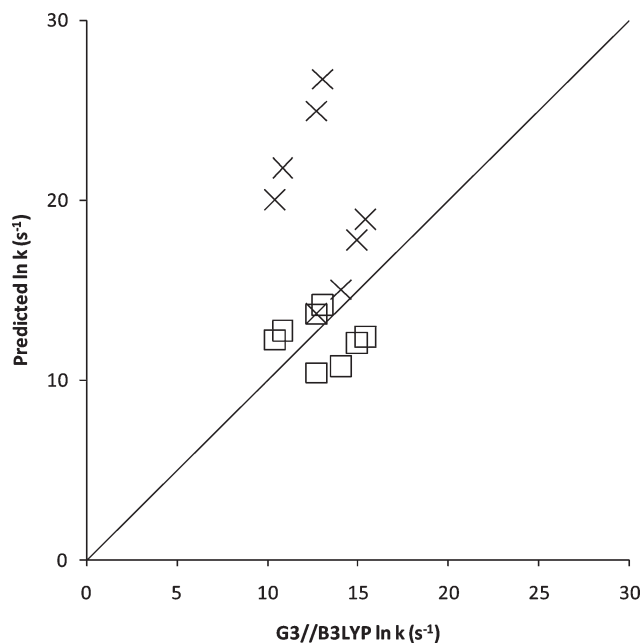


Figure 11. Parity plot of Si_2H_2 elimination rate coefficients for the reactions in Figure 2 and Figure 3. The open squares are for the rate coefficients of the reactions of Figure 2 and Figure 3 predicted with the revised Evans–Polanyi correlation parameters of Table 6. Rate coefficients predicted by the current literature correlations for monofunctional substituted silylene elimination reaction kinetics for silicon hydrides are shown with crosses.

substituents are added to the saturated silicon hydride that ultimately donates a hydrogen atom to the Si_2H_2 isomer, they do not change the structure of the reactive center significantly. When only one silyl substituent is added to the reactive center (Figure 9), most of the effects on the reactive center and subsequent kinetic parameters are electronic.

It is clear that the reactive center and consequently the kinetic parameters vary uniformly with systematic variation in the connectivity of the reactive center, making the Si_2H_2 and potentially Si_2R_2 isomers, where R is a silicon-based substituent and/or part of a ring, great candidates for linear free energy relationships, e.g., the Evans–Polanyi correlation in eq 5, or transition state group additivity methods^{40–43} to predict kinetic parameters. However, the direct products of the insertion reactions of bridged Si_2H_2 isomers into monosilane and disilane are hydrogen-bridged species. These species are not the final stable product upon which the enthalpy of reaction used in classic kinetic correlations (e.g., the Evans–Polanyi correlation) for addition reactions with monofunctional silicon hydrides are typically based. That is, the 1,2-hydrogen bridged species can isomerize to a silene or silylene that are both lower in energy, and the silene and the silylene can then isomerize to a three-membered ring that is lower in energy by passing through a 1,3-hydrogen bridged intermediate.^{40,42} Therefore, it is appealing to develop kinetic correlations that encompass reactants and

products on which current thermodynamic property and kinetic parameter databases are typically based.

In Figure 10, the activation energies obtained from our quantum chemical calculations for all reactions in Figure 2 and Figure 3 and activation energies predicted by the available literature correlation for monofunctional substituted silylene addition and elimination are plotted as a function of the standard enthalpy of reaction. Monofunctional substituted silylene addition reactions have Evans–Polanyi parameters of $\tilde{A} = 2 \times 10^{15} \text{ s}^{-1}$ (elimination)^{18,76} and $E_o = 0$ and $\alpha = 0$ (addition) and $\alpha = 1$ (elimination), which were generalized from reactions composed of two to three silicon atoms.^{19,77} The plot of activation energies as a function of the standard enthalpy of reaction for the reactions of this study reveals two interesting results. First, the literature correlation based on monofunctional species is clearly an inadequate description of the relationship between E_a and ΔH_{rxn} for the addition of multifunctional species. Second, all eight of the reactions can clearly be captured very well by only one set of Evans–Polanyi parameters. The Evans–Polanyi parameters, i.e., α_{addition} , $\alpha_{\text{elimination}}$, and E_o , were calculated from linear regression with the least-squares method subject to parameter constraints to maintain enthalpic consistency (Figure 10). The constraints for enthalpic consistency were (1) $\alpha_{\text{addition}} + \alpha_{\text{elimination}} = 1$, and (2) E_o is the same for the addition and elimination reactions. The Evans–Polanyi parameters are summarized for Si_2H_2 addition and elimination reaction kinetics under pyrolysis conditions in Table 6. The average absolute error between the activation energies regressed from G3//B3LYP rate coefficients and the activation energies predicted with the new Evans–Polanyi correlations using the regressed parameters from our study for all reactions was approximately 1.2 kcal mol⁻¹. It is clear that the ability of the revised Evans–Polanyi correlations to capture the activation energies from G3//B3LYP is superior to that of the available literature correlations for monofunctional substituted silylene addition and elimination.

When pre-exponential factors using the reaction family concept are estimated, pre-exponential factors are usually given as a representative or average value for a given reaction family. For the rigorous estimation of pre-exponential factors, a method, such as the transition state group additivity approach employed in our previous work on monofunctional silicon hydride reaction families, is recommended.^{40–43} However, this group additivity method requires a large set of reactions and is beyond the scope of this study. Specification of one pre-exponential factor for elimination from all of the reactions in this study is recommended. The average $\log \tilde{A}$ value for elimination of all reactions in this study is 13.6 (where \tilde{A} has units of s^{-1}).

It was next interesting to examine how well the reaction family concept and the associated kinetic correlations used for molecules with a single functional group perform for predicting rate coefficients of multifunctional elimination reactions and how well the new kinetic correlations perform. When extended to all of the reactions in this study, the average absolute ratio between the rate coefficients calculated using activation energies estimated from the original Evans–Polanyi relationship and the representative pre-exponential factor based on monofunctional substituted silylene elimination and those from G3//B3LYP was nearly 1×10^5 . Using the revised Evans–Polanyi correlations in Table 6 and a representative pre-exponential factor of $3.8 \times 10^{13} \text{ s}^{-1}$, the sum of squared error between the predicted rate coefficients and the G3//B3LYP values was significantly lower. A parity plot depicting how well the revised Evans–Polanyi

correlations and a representative pre-exponential factor capture the rate coefficients regressed from G3//B3LYP for Si_2H_2 elimination reactions is shown in Figure 11. The values predicted from the kinetic correlations in the literature for monofunctional substituted silylene elimination are also provided for comparison. The superiority of the revised Evans–Polanyi correlations and the representative pre-exponential factor is even more clearly demonstrated when the A and E_a values are examined individually (Table S). Thus, the predictive capability of the revised Evans–Polanyi correlations and the representative \tilde{A} value over a wide range of A and E_a values is preferred in the calculation of rate coefficients for multifunctional addition and elimination reactions. A representative pre-exponential factor for the reverse rate coefficient for addition is not required because the rate coefficient is calculated from the Gibbs free energy of reaction based on the principle of thermodynamic reversibility.

Our results give detailed information about the reaction kinetics of multifunctional species, with higher reactivities observed for the unbridged isomers because of restrictive kinetic bottlenecks for the reaction of bridged (or stabilized) Si_2H_2 isomers with SiH_4 and Si_2H_6 . Although beyond the scope of this study, the detailed mapping of the reaction kinetics of multifunctional silicon hydrides larger than Si_2H_2 is particularly important and recommended. These larger multifunctional silicon hydrides can form singly hydrogen-bridged structures analogous to the $\text{Si}(\text{H})\text{SiH}$ isomer of Si_2H_2 but cannot form dibridged structures analogous to the $\text{Si}(\text{H}_2)\text{Si}$ isomer of Si_2H_2 .

CONCLUSIONS

Rate coefficients and Arrhenius parameters for the addition and elimination reactions between the four isomers of Si_2H_2 , SiH_4 , and Si_2H_6 were calculated using G3//B3LYP, statistical thermodynamics, conventional and variational transition state theory, and internal rotation corrections. The overall reaction of *trans*-HSiSiH addition to a saturated silicon hydride was found to pass through a concerted transition state via positive activation energy to produce a substituted silylene. For addition of $\text{Si}(\text{H})\text{SiH}$ or $\text{Si}(\text{H}_2)\text{Si}$ to a saturated silicon hydride, the overall reaction was found to pass through a concerted transition state via positive activation energy to produce a monobridged intermediate. The overall reaction of SiSiH₂ addition to a saturated silicon hydride was found to pass through a stable adduct that decomposes via an exothermic reaction to produce a silene. For SiSiH₂ addition reactions, the rate-determining step was determined to be from the reactants to the adduct under pyrolysis conditions, and then kinetic parameters for the overall reaction were calculated to align better with mechanistic modeling efforts. The Si_2H_2 isomers were found to be more reactive on average with Si_2H_6 than SiH_4 because the products formed from the addition to SiH_4 lack the electron delocalization and subsequent stabilization of the divalent center or double bond present in the larger products formed from the addition to Si_2H_6 . Revised parameters for the Evans–Polanyi correlation and a representative pre-exponential factor were developed for Si_2H_2 addition and elimination reaction families under pyrolysis conditions from the reactions in this study and found to capture the activation energies and rate coefficients very well. The revised parameters for the Evans–Polanyi correlation and a representative pre-exponential factor outperform the current literature methods generalized from monofunctional substituted silylene elimination for the prediction of Si_2H_2 elimination rate coefficients.

■ ASSOCIATED CONTENT

S Supporting Information. Rate coefficients of all addition and elimination reactions (Table S1). External symmetry numbers, internal symmetry numbers for noncanceling internal rotations treated as free rotations, and number of chiral isomers for all species (Table S2). B3LYP/6-31G(d) geometries and frequencies for all Si₂H₂ isomers, substituted silylenes, silenes, silanes, hydrogen-bridged intermediates, and rate-determining transition states (Table S3). Rate coefficients for reactions 2 and 6 used in the full microkinetic model (Table S4). Product silene concentration as a function of time and temperature for reaction 2 (Figure S1) and reaction 6 (Figure S2). B3LYP/6-31G(d) transition state geometries for the second step in the addition direction for reactions 2 and 6 (Figure S3). Potential energy surfaces for reactions 2 and 6 (Figure S4). This material is available free of charge via the Internet at <http://pubs.acs.org.org>.

■ AUTHOR INFORMATION

Corresponding Author

*Fax: (+1)847-491-3728. E-mail: broadbelt@northwestern.edu.

■ ACKNOWLEDGMENT

We are grateful for the support of this work by the following organizations: (1) National Science Foundation (Collaborative Research Grant CBET-0500320 and NCSA Teragrid Supercomputing Facilities) and (2) ARCS Foundation Inc.

■ REFERENCES

- (1) Jasinski, J. M.; Meyerson, B. S.; Scott, B. A. *Annu. Rev. Phys. Chem.* **1987**, *38*, 109–140.
- (2) Becerra, R.; Walsh, R. *J. Phys. Chem.* **1992**, *96*, 10856–10862.
- (3) Onischuk, A. A.; Strunin, V. P.; Ushakova, M. A.; Panfilov, V. N. *Int. J. Chem. Kinet.* **1998**, *30*, 99–110.
- (4) Zheng, W.; Gallagher, A. *Thin Solid Films* **2008**, *516*, 929–939.
- (5) Nakamura, S.; Matsumoto, K.; Susa, A.; Koshi, M. *J. Non-Cryst. Solids* **2006**, *352*, 919–924.
- (6) Holt, J. K.; Swiatek, M.; Goodwin, D. G.; Muller, R. P.; Goddard, W. A.; Atwater, H. A. *Thin Solid Films* **2001**, *395*, 29–35.
- (7) Nakamura, S.; Matsugi, A.; Susa, A.; Koshi, M. *Thin Solid Films* **2008**, *516*, 517–520.
- (8) Lischka, H.; Kohler, H. J. *J. Am. Chem. Soc.* **1983**, *105*, 6646–6649.
- (9) Truhlar, D. G.; Gordon, M. S. *Science* **1990**, *249*, 491–498.
- (10) Binkley, J. S. *J. Am. Chem. Soc.* **1984**, *106*, 603–609.
- (11) Koseki, S.; Gordon, M. S. *J. Phys. Chem.* **1989**, *93*, 118–125.
- (12) Koseki, S.; Gordon, M. S. *J. Phys. Chem.* **1988**, *92*, 364–367.
- (13) Curtiss, L. A.; Raghavachari, K.; Deutsch, P. W.; Pople, J. A. *J. Chem. Phys.* **1991**, *95*, 2433–2444.
- (14) Sannigrahi, A. B.; Nandi, P. K. *Chem. Phys. Lett.* **1992**, *188*, 575–583.
- (15) Colegrove, B. T.; Schaefer, H. F. *J. Phys. Chem.* **1990**, *94*, 5593–5602.
- (16) Grev, R. S.; Schaefer, H. F. *J. Chem. Phys.* **1992**, *97*, 7990–7998.
- (17) O'Farrell, N.; Houlton, A.; Horrocks, B. R. *Int. J. Nanomed.* **2006**, *1*, 451–472.
- (18) Swihart, M. T.; Girshick, S. L. *J. Phys. Chem. B* **1999**, *103*, 64–76.
- (19) Wong, H. W.; Li, X. G.; Swihart, M. T.; Broadbelt, L. J. *J. Phys. Chem. A* **2004**, *108*, 10122–10132.
- (20) Wong, H. W.; Nieto, J. C. A.; Swihart, M. T.; Broadbelt, L. J. *J. Phys. Chem. A* **2004**, *108*, 874–897.
- (21) Nakajima, Y.; Tonokura, K.; Sugimoto, K.; Koshi, M. *Int. J. Chem. Kinet.* **2001**, *33*, 136–141.
- (22) Dollet, A.; de Persis, S. *J. Anal. Appl. Pyrolysis* **2007**, *80*, 460–470.
- (23) Koi, M.; Tonokura, K.; Tezaki, A.; Koshi, M. *J. Phys. Chem. A* **2003**, *107*, 4838–4842.
- (24) Dickinson, A. P.; Oneal, H. E.; Ring, M. A. *Organometallics* **1991**, *10*, 3513–3520.
- (25) Hu, S. W.; Wang, Y.; Wang, X. Y.; Chu, T. W.; Liu, X. Q. *J. Phys. Chem. A* **2003**, *107*, 2954–2963.
- (26) Mick, H. J.; Markus, M. W.; Roth, P.; Smirnov, V. N. *Ber. Bunsen-Ges. Phys. Chem. Chem. Phys.* **1995**, *99*, 880–890.
- (27) Matsumoto, K.; Koshi, M. *J. Electrochem. Soc.* **2008**, *155*, D419–D423.
- (28) Baboul, A. G.; Curtiss, L. A.; Redfern, P. C.; Raghavachari, K. *J. Chem. Phys.* **1999**, *110*, 7650–7657.
- (29) Katzer, G.; Sax, A. F. *J. Comput. Chem.* **2005**, *26*, 1438–1451.
- (30) Katzer, G.; Sax, A. F. *Chem. Phys. Lett.* **2003**, *368*, 473–479.
- (31) Katzer, G.; Sax, A. F. *J. Phys. Chem. A* **2002**, *106*, 7204–7215.
- (32) Ayala, P. Y.; Schlegel, H. B. *J. Chem. Phys.* **1998**, *108*, 2314–2325.
- (33) Pfaendtner, J.; Yu, X.; Broadbelt, L. J. *Theor. Chem. Acc.* **2007**, *118*, 881–898.
- (34) Van Speybroeck, V.; Vansteenkiste, P.; Van Neck, D.; Waroquier, M. *Chem. Phys. Lett.* **2005**, *402*, 479–484.
- (35) Vansteenkiste, P.; Van Speybroeck, V.; Marin, G. B.; Waroquier, M. *J. Phys. Chem. A* **2003**, *107*, 3139–3145.
- (36) Ashcraft, R. W.; Green, W. H. *J. Phys. Chem. A* **2008**, *112*, 9144–9152.
- (37) Catoire, L.; Swihart, M. T.; Gail, S.; Dagaut, P. *Int. J. Chem. Kin.* **2003**, *35*, 453–463.
- (38) Frisch, M. J.; Trucks, G. W.; Schlegel, H. B.; Scuseria, G. E.; Robb, M. A.; Cheeseman, J. R.; Montgomery Jr., J. A.; Vreven, T.; Kudin, K. N.; Burant, J. C.; Millam, J. M.; Iyengar, S. S.; Tomasi, J.; Barone, V.; Mennucci, B.; Cossi, M.; Scalmani, G.; Rega, N.; Petersson, G. A.; Nakatsuji, H.; Hada, M.; Ehara, M.; Toyota, K.; Fukuda, R.; Hasegawa, J.; Ishida, M.; Nakajima, T.; Honda, Y.; Kitao, O.; Nakai, H.; Klene, M.; Li, X.; Knox, J. E.; Hratchian, H. P.; Cross, J. B.; Bakken, V.; Adamo, C.; Jaramillo, J.; Gomperts, R.; Stratmann, R. E.; Yazyev, O.; Austin, A. J.; Cammi, R.; Pomelli, C.; Ochterski, J. W.; Ayala, P. Y.; Morokuma, K.; Voth, G. A.; Salvador, P.; Dannenberg, J. J.; Zakrzewski, V. G.; Dapprich, S.; Daniels, A. D.; Strain, M. C.; Farkas, O.; Malick, D. K.; Rabuck, A. D.; Raghavachari, K.; Foresman, J. B.; Ortiz, J. V.; Cui, Q.; Baboul, A. G.; Clifford, S.; Cioslowski, J.; Stefanov, B. B.; Liu, G.; Liashenko, A.; Piskorz, P.; Komaromi, I.; Martin, R. L.; Fox, D. J.; Keith, T.; Al-Laham, M. A.; Peng, C. Y.; Nanayakkara, A.; Challacombe, M.; Gill, P. M. W.; Johnson, B.; Chen, W.; Wong, M. W.; Gonzalez, C.; Pople, J. A. *Gaussian 03, Revision D.01*, Gaussian, Inc., Wallingford, CT, 2004.
- (39) Martin, J. M. L.; de Oliveira, G. *J. Chem. Phys.* **1999**, *111*, 1843–1856.
- (40) Adamczyk, A. J.; Reyniers, M. F.; Marin, G. B.; Broadbelt, L. J. *Theor. Chem. Acc.* **2011**, *128*, 91–113.
- (41) Adamczyk, A. J.; Reyniers, M. F.; Marin, G. B.; Broadbelt, L. J. *ChemPhysChem* **2010**, *11*, 1978–1994.
- (42) Adamczyk, A. J.; Reyniers, M.-F.; Marin, G. B.; Broadbelt, L. J. *J. Phys. Chem. A* **2009**, *113*, 10933–10946.
- (43) Adamczyk, A. J.; Reyniers, M. F.; Marin, G. B.; Broadbelt, L. J. *Phys. Chem. Chem. Phys.* **2010**, *12*, 12676–12696.
- (44) Jursic, B. S. *J. Mol. Struct.* **1999**, *459*, 221–228.
- (45) Jalbout, A. F.; Swihart, M. T.; Jursic, B. S. *J. Mol. Struct. (THEOCHEM)* **2001**, *571*, 231–232.
- (46) Scott, A. P.; Radom, L. *J. Phys. Chem.* **1996**, *100*, 16502–16513.
- (47) Henkelman, G.; J., H. *J. Chem. Phys.* **2000**, *113*, 9978–9985.
- (48) Henkelman, G.; U., B. P.; Jonsson, H. *J. Chem. Phys.* **2000**, *113*, 9901–9904.
- (49) Jonsson, H.; Mills, G.; Jacobsen, K. W. In *Classical and Quantum Dynamics in Condensed Phase Simulations*; World Scientific: Singapore, 1998; pp 385–404.
- (50) McQuarrie, D. A.; Simon, J. D. *Molecular Thermodynamics*; University Science Book: Sausalito, CA, 1999.

- (51) Hirschfelder, J. O.; Wigner, E. *J. Chem. Phys.* **1939**, *7*, 616–628.
- (52) Fernandez-Ramos, A.; Ellingson, B. A.; Meana-Paneda, R.; Marques, J. M. C.; Truhlar, D. G. *Theor. Chem. Acc.* **2007**, *118*, 813–826.
- (53) Truhlar, D. G.; Garrett, B. C. *Annu. Rev. Phys. Chem.* **1984**, *35*, 159–189.
- (54) Evans, M. G.; Polanyi, M. *Trans. Farad. Soc.* **1938**, *34*, 11–29.
- (55) Moore, J. W.; Pearson, R. G. *Kinetics and Mechanism*, 3rd ed.; John Wiley: New York, 1981.
- (56) Petrov, K. T.; Veszpremi, T. *Int. J. Quantum Chem.* **2009**, *109*, 2526–2541.
- (57) Cerofolini, G. F.; Giorgi, G.; Sgamellotti, A.; Belanzoni, P. *J. Chem. Phys.* **2009**, *130* (10), 184702–184702–10.
- (58) Owens, Z. T.; Larkin, J. D.; Schaefer, H. F. *J. Chem. Phys.* **2006**, *125*, 164322–164322–7.
- (59) Yamaguchi, Y.; Deleeuw, B. J.; Richards, C. A.; Schaefer, H. F.; Frenking, G. *J. Am. Chem. Soc.* **1994**, *116*, 11922–11930.
- (60) Deleeuw, B. J.; Grev, R. S.; Schaefer, H. F. *J. Chem. Educ.* **1992**, *69*, 441–444.
- (61) Wiberg, K. B. *Tetrahedron* **1968**, *24*, 1083–1096.
- (62) Becerra, R.; Frey, H. M.; Mason, B. P.; Walsh, R.; Gordon, M. S. *J. Am. Chem. Soc.* **1992**, *114*, 2151–2752.
- (63) McCarthy, M. C.; Yu, Z.; Sari, L.; Schaefer, H. F.; Thaddeus, P. *J. Chem. Phys.* **2006**, *124*, 7.
- (64) Rappoport, Z.; Apeloig, Y. *The Chemistry of Organic Silicon Compounds*; Wiley: New York, 1998; Vol. 2, Chapter 43.
- (65) Van Speybroeck, V.; Van Neck, D.; Waroquier, M. *J. Phys. Chem. A* **2002**, *106*, 8945–8950.
- (66) East, A. L. L.; Radom, L. *J. Chem. Phys.* **1997**, *106*, 6655–6674.
- (67) Wong, B. M.; Green, W. H. *Mol. Phys.* **2005**, *103*, 1027–1034.
- (68) Mozurkewich, M.; Benson, S. W. *J. Phys. Chem.* **1984**, *88*, 6429–6435.
- (69) Fukui, K. *Science* **1982**, *218*, 747–754.
- (70) Aird, R. W. S.; Canosamas, C. E.; Cook, D. J.; Marston, G.; Monks, P. S.; Wayne, R. P.; Ljungstrom, E. *J. Chem. Soc., Farad. Trans.* **1992**, *88*, 1093–1099.
- (71) King, M. D.; Canosa-Mas, C. E.; Wayne, R. P. *Phys. Chem. Chem. Phys.* **1999**, *1*, 2231–2238.
- (72) Bader, R. F. W. *Can. J. Chem.-Rev. Can. Chim.* **1962**, *40*, 1164–1175.
- (73) Street, R. A. *Hydrogenated Amorphous Silicon*; Cambridge University Press: Cambridge, 1991.
- (74) Willems, P. A.; Froment, G. F. *Ind. Eng. Chem. Res.* **1988**, *27*, 1966–1971.
- (75) Willems, P. A.; Froment, G. F. *Ind. Eng. Chem. Res.* **1988**, *27*, 1959–1966.
- (76) Ho, P.; Coltrin, M. E.; Breiland, W. G. *J. Phys. Chem.* **1994**, *98*, 10138–10147.
- (77) Girshick, S. L.; Swihart, M. T.; Suh, S. M.; Mahajan, M. R.; Nijhawan, S. *J. Electrochem. Soc.* **2000**, *147*, 2303–2311.